COMPARATIVE STUDY ON THE PULL-OUT RESPONSE OF NONWOVEN GEOTEXTILE IN DRY AND SATURATED SANDS

Ching-Chuan Huang [1*], Shih-Cieh Yin [2], and Hao-Yi Hsu [2]

ABSTRACT

A series of pull-out tests is performed to investigate the response of a heat-bonded nonwoven geotextile under both dry and saturated conditions. Modeling of the pull-out behavior for the dry and saturated sand conditions is also conducted based on a hyperbolic curve-fitting technique. A theory regarding the effective pull-out lengths in conjunction with the result of medium-scale direct shear tests on the soil-geotextile interface is used to facilitate the modeling for the pull-out force *vs.* displacement relationships. Test results show that both the peak pull-out strength and its associated pull-out displacement are lower in the case of saturated sand than those in dry sands due to the lubrication effect of water. The soil-saturation-induced different pull-out behavior is reflected in three key model parameters in the hyperbolic pull-out model. The hyperbolic pull-out model established here successfully simulates the observed behavior in terms of the initial stiffness, the peak pull-out resistance and its associated pull-out displacement for the tests with a pull-out failure mode. For the tests exhibiting tie-break failure, the proposed model tends to under-estimate the pull-out displacement at failure due to a lack of consideration for the tensile elongation of the tested geotextile.

Key words: Geosynthetics, pull-out, hyperbolic model, interface frition angle, dry sand, saturated sand.

1. INTRODUCTION

The soil-geosynthetic interface bonding property is one of the key factors to be considered in the design and analyses of geosynthetic-reinforced soil structures. To this end, pull-out tests have been conducted to obtain a so-called "bonding coefficient" in order to facilitate internal stability analyses (*e.g.*, Berg *et al.* 2009; Palmeira 2009; Pinho-Lopes *et al.* 2015). The lump-summed "bonding coefficient" is a simplistic design parameter for which non-linear stresses (or strains) along the pull-out specimen are ignored (Palmeira 2009; Yang *et al.* 2012). To overcome this drawback, both analytical and experiment-based methods have been proposed to predict the pull-out behavior of a heat-bonded nonwoven geotextile (Weerasekara and Wijewichreme 2010; Huang *et al.* 2014). On the other hand, the direct shear test which is characterized by an "element test" nature has also been widely used to derive soil-geotextile interface shear strengths (Krahn *et al.* 2007; Liu *et al.* 2009; Vieira *et al.* 2013; Bacas *et al.* 2015; Ferreira *et al.* 2015; Verira and Pereira 2015). These strength parameters, including the adhesion, the friction angle, the initial stiffness, and the failure envelope, have been widely used to simulate the non-linear (or non-uniform) response of geotextiles in reinforced soil structures. A direct use of interface strength parameters obtained in direct shear tests in limit-equilibrium-based designs requires an empirical reduction factor for the evaluated pull-out resistance to account for the non-linear

stress distribution along the geosynthetic reinforcement. An alternative approach to take into account the above-mentioned non-linear behavior is to use a so-called "effective (or active) pull-out length," as proposed by Huang *et al.* (2014) and Gardile *et al.* (2016). Huang *et al.* (2014) incorporated a back-calculated soil-reinforcement interface friction angle to derive the effective pull-out length for a heat-bonded nonwoven geotextile in order to facilitate displacement analyses for geosynthetic-reinforced slopes. Gardile *et al.* (2016) performed large-scale pull-out tests on two high-stiffness geogrids embedded in dry, cohesionless sand. They showed that the active pull-out lengths of geogrids increased with increases in the pull-out load, up to the moment of pull-out failure. They also showed that the active pull-out lengths of geogrids are a function of geogrid tensile rigidities, overburden pressures, specimen lengths, and applied loads.

The above-mentioned studies on the pull-out and direct shear behavior of soil-geosynthetics interfaces were all conducted using dry soil medium. However, soil structures are often exposed to rainfall and groundwater seepage, so a concern arises regarding the validity of using the soil-reinforcement interface properties obtained in the tests of dry soils, especially when significant pull-out strength loss is expected under saturated environmental conditions. Studies focused on comparisons of the behavior of dry and saturated reinforced soil structures are very limited in number (Pathak and Alfaro 2010; Portelinha *et al.* 2013; Huang 2015a; Yang *et al.* 2016).

2. PULL-OUT TEST SET-UP

Figure 1 shows the pull-out test system consisting of a steel pull-out box 350 mm wide, 350 mm deep, and 250 mm long, a diaphragm air cylinder and an air pressure regulator for applying confining pressures, a water tank for specimen saturation, and a

Fig. 1   Side-view of the pull-out system

Fig. 2   Geometrical details of the pull-out box
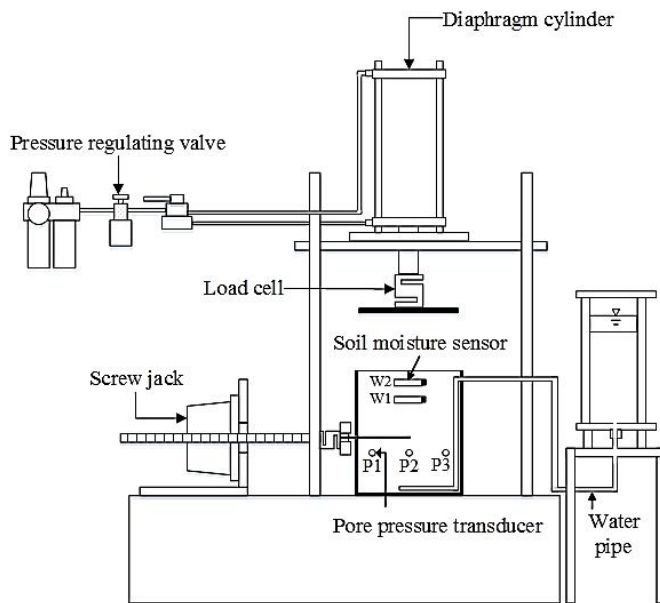
screw jack and pull-out grip for applying constant-displacement-rate pull-out. The geometrical details of the pull-out box and the deployment of the porewater pressure sensors (P1, P2, and P3) and moisture sensors (W1 and W2) are shown in Fig. 2. A sandy soil classified as SP according to the Unified Soil Classification System (USCS; ASTM D2487) is used as the test medium. The soil used here is a river sand with a specific gravity (G_s) of 2.63 and a mean particle size (D_{50}) of 0.213 mm; the particle size with 10% of finer (D_{10}) is 0.08 mm; the particle size with 85% finer (D_{85}) is 0.5 mm; the maximum particle size (D_{max}) is 2.0 mm which has been extensively used as the test medium in previous studies conducted by the author (Huang *et al.* 2008; 2009; Huang 2015a). Note that the pull-out box used here is not a standard testing device such as that proposed by ASTM D6706 which is intended to be a performance test conducted to replicate design or as-built condition. Nevertheless, the pull-out box used in the present study meets the boundary condition requirements proposed by ASTM D6706: (1) The minimum width is the greater of 20 times of the particle size with 85% finer, D_{85} (= 20 × 0.5 = 10 mm), or 6 times of the maximum particle size of the soil, D_{max} (= 6 × 2.0 = 12 mm); (2) the box allows for a minimum depth of 150 mm above and below the geosynthetics; (3) the depth of the soil in the box above or below the geosynthetics is large than the greater of 6 times of D_{85} (= 6 × 0.5 = 3.0 mm) or 3 times of D_{max} (= 3 × 2.0 = 6 mm) of the soil.

For the pull-out tests reported here, sands were oven-dried before use and were compacted to a specific dry density (γ_d) of 15 kN/m^3, which has either a relative density (D_r) of 62% or a void ratio of 0.67. The compaction procedure consists of (1) spreading evenly a specific quantity of air-dried sands which is to achieve a specific targeted dried unit weight for a compaction lift of 10 mm high in a 300 mm × 300 mm pull-out box; (2) placing a 10 mm thick, 100 mm × 100 mm steel plate over the top of the spread sand; (3) lifting the steel plate to specific heights of 0 ~ 10 mm, depending on the targeted density, and dropping the steel plate on the top of compacted sand till the sand surface flushes
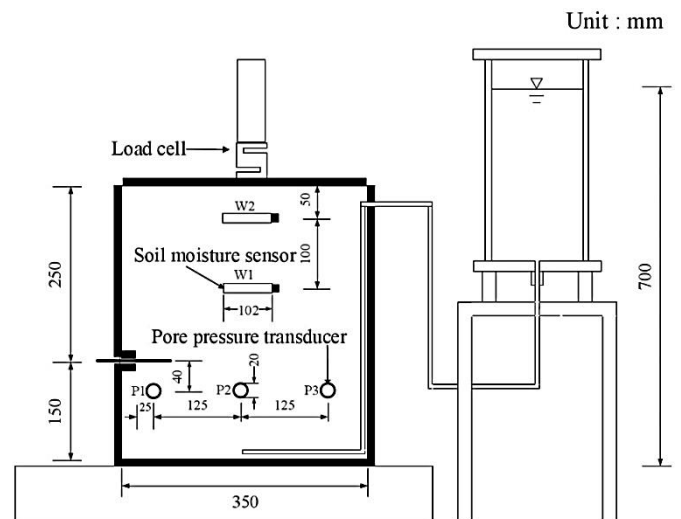
with the target line printed on the side wall of pull-out box; (4) repeating steps (2) and (3), till the sand surface of the compacted sands flushed with the target line on the side-wall. For the tests using saturated sands, de-air water was supplied from a water tank as shown in Fig. 1 through a perforated de-air water pipe installed at the bottom of the sand specimen. To prevent the leakage of de-aired water through the pull-out slit, two rubber sheets were plugged in the slit as a temporary sealer which are removed immediately before the pull-out tests. Degrees of soil saturation were detected by the soil moisture sensors set at 50 and 100 mm in the pull-out box. In all of the tests reported here, the degree of saturation at the end of the saturation process, $S_r \geq$ 94%, was confirmed using the method proposed by Huang *et al.* (2008, 2009). The stress-strain curves for the geotextile pull-out specimen using a wide-width tensile test apparatus are shown in Fig. 3(a). The pull-out specimen was a heat-bonded nonwoven geotextile which has an ultimate tensile strength (T_{ult}) of 4.1 kN/m, a break elongation (ε_f) of 37%, and secant moduli at 2% ($J_{2\%}$) and 5% ($J_{5\%}$) of 70 and 36 kN/m, respectively, according to a standard wide-width tensile test method (ASTM D4595). The nonwoven geotextile with $J_{2\%}$ = 70 kN/m was intended to be used as the reinforcement in a 0.5m-high reduced-scale model slope. The nonwoven geotextile used here mimics a geotextile reinforcement with $J_{2\%}$ = 70 × 10^2 = 7000 kN/m in a 5m-high proto-type reinforced slope, based on a similitude proposed by Huang (2016b). A reinforcing material with $J_{2\%}$ = 7000 kN/m can be categorized as a high-stiffness geosynthetic reinforcement, such as woven multifilament geotextiles, based on the classification system provided by Shukla (2002). Therefore, modeling of pull-out behavior of geosynthetics reported here is to simulate the pull-out behavior of a reinforcement in model tests, not to create a generalized pull-out model for variety of soil and reinforcement conditions. A large-strain type strain gauge (YFLA-20; Tokyo-sokki Co., Japan) with a limit strain of 10% ~ 15% was used to measure the tensile strains of the geotextile during the pull-out tests. Calibration for the strain gauges attached to the geotextile was performed to derive the strain gauge output *vs.* the wide-width tensile strain relationships, as shown in Fig. 3(b). The output signals from the strain gauges during the tests were first converted to the wide-width tensile strains based on Fig. 3(b) which were in-turn converted to the tensile forces based on Fig. 3(a).
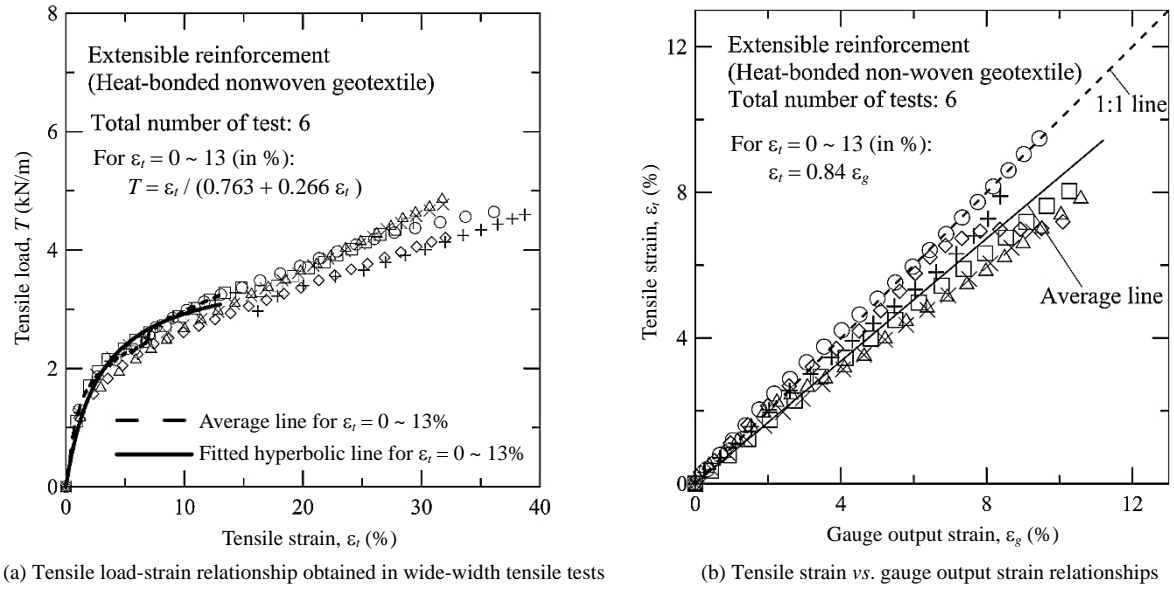
(a) Tensile load-strain relationship obtained in wide-width tensile tests

(b) Tensile strain *vs.* gauge output strain relationships

Fig. 3   Characteristics of the heat-bonded nonwoven geotextile

3. RESULTS OF PULL-OUT TESTS ON DRY SAND

Figures 4(a) to 4(c) show the pull-out force (T) *vs.* displacement (Δ) relationships for $L_t = 50$, 75, and 100 mm, respectively (L_t: Total length of pull-out specimen). In the case of a short embedment length ($L_t = 50$ mm), a pull-out failure mode prevails despite the changes in confining pressures from 20 to 100 kPa. A typical example of pull-out failure observed in the test is shown in Fig. 5(a) in which the geotextile specimen is drawn from the box with a rather limited tensile elongation. The values of pull-out displacement (Δ_f) required for reaching peak pull-out forces (T_f) increase with increases in confining stresses. The above trends are slightly changed for the case of $L_t = 75$ mm, as shown in Fig. 4(b), *i.e.*, a tie-break failure occurred in the case of a high effective confining pressure ($\sigma_n' = 100$ kPa). Comparing Figs. 4(a) and 4(b), an overall increase in the values of Δ_f can be seen in the case of $L_t = 75$ mm, as a result of tensile elongations along the length of the embedment. In the case of $L_t = 100$ mm, as shown in Fig. 4(c), the tie-break failure mode is dominant except in the case with a low confining pressure of $\sigma_n' = 20$ kPa. A typical example of tie-break failure is shown in Fig. 5(b) in which an excessive elongation prior to the tensile failure of the geotextile can be seen.
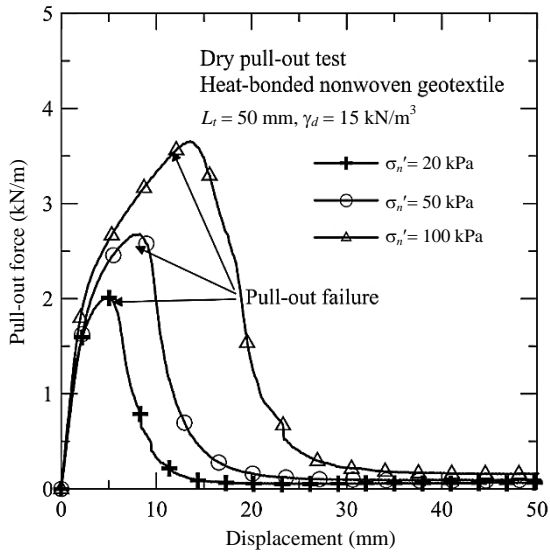
4. RESULTS OF PULL-OUT TESTS ON SATURATED SAND

Figures 6(a) to 6(c) show the T *vs.* Δ relationships under similar test conditions as those shown in Figs. 4(a) to 4(c), except that these pull-out tests are conducted under fully saturated environmental conditions. Figure 6(a) shows the T *vs.* Δ relationships for the tests of $L_t = 50$ mm. An overall trend similar to that shown in the dry case (as shown in Fig. 4(a)) can be seen, except that the values of Δ_f are smaller than those for the dry sand. For the case of $L_t = 75$ mm, as shown in Fig. 6(b), an overall trend of in-
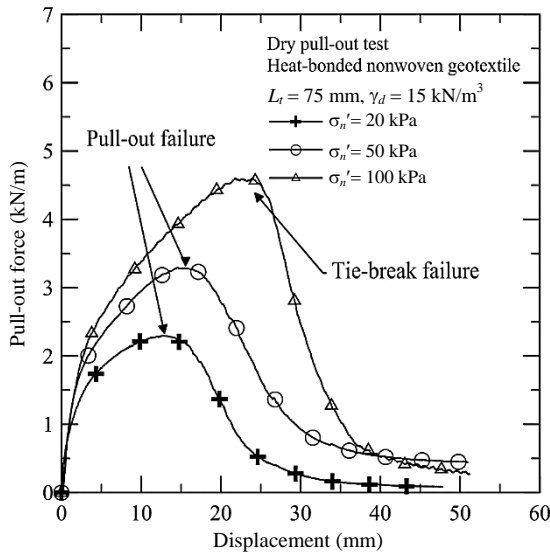
creased Δ_f with the increase of σ_n' can be seen. This trend is identical to that observed under dry conditions, as discussed in Fig. 4(b), except that in the case of saturated sands, pull-out failure is an exclusive mode. Figure 6(c) shows that tie-break failures occur for higher σ_n' (= 50 and 100 kPa), which are similar to those shown in the dry cases, as discussed in Fig. 4(c). Comparing Figs. 4(a) and 6(a), soil saturation seems to play the role of a lubricant, which causes measurable decreases in T_f and Δ_f. This is also true for the pull-out specimen length of $L_t = 75$ mm (comparing Figs. 4(b) and 6(b)). The above-mentioned trend is not clear in the case of $L_t = 100$ mm because in this case, excessive elongation of the geotextile adjacent to the clamp also contributes to the pull-out displacement.

5. MEASURED NON-UNIFORM STRAIN DISTRIBUTIONS ALONG THE PULL-OUT SPECIMEN
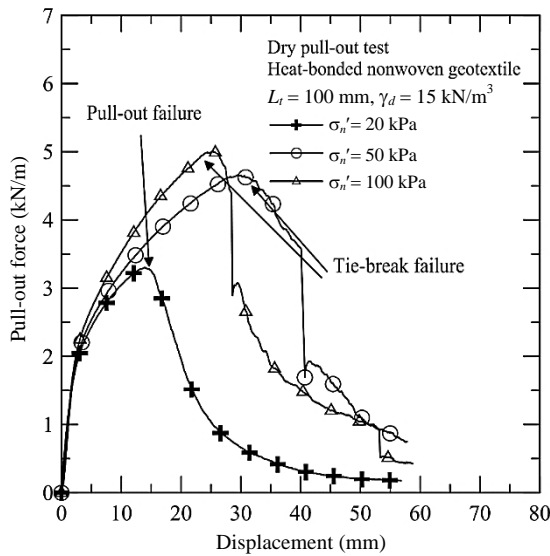
Figures 7(a) and 7(b) show the tensile strains measured at various locations from the pull-out face for dry and saturated conditions, respectively. In Fig. 7(a), two distinctive groups of curves can be seen, *i.e.*, those for $d = 25$ mm (d: The location of strain gauge from the pull-out face) and those for $d = 55$ mm. In addition, pull-out-induced tensile strains mobilize more effectively at $d = 25$ mm than is the case at $d = 55$ mm, regardless of the values of σ_n'. A majority of these curves show flat-to-steep transitions at $\Delta = 10$ and 30 mm, except the one with $\sigma_n' = 100$ kPa. The value of Δ at which an abrupt strain transition is detected increases with increases in σ_n' suggesting that the pull-out-induced tensile strains mobilize more easily under low values of σ_n'. This also implies that the effective pull-out length (or the active pull-out length) decreases with increases in σ_n', as shown in Eqs. (7) and (8) (to be discussed later). A different pull-out behavior from that shown in the dry case (Fig. 7(a)) can be seen in the saturated case (Fig. 7(b)), *i.e.*, values of Δ_f at the location of $d = 25$ mm are generally smaller in the saturated case than
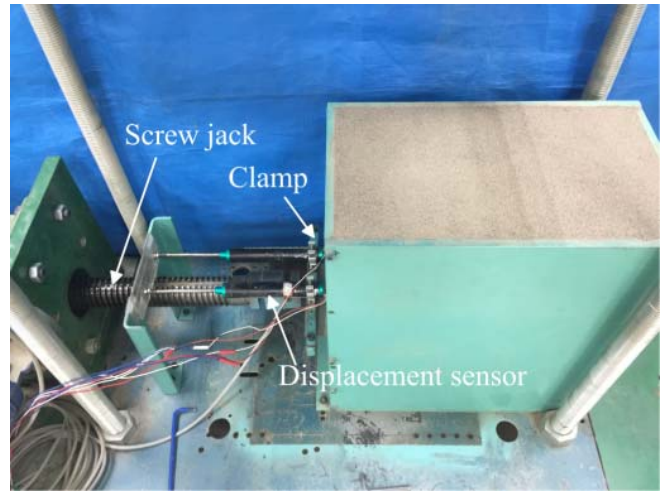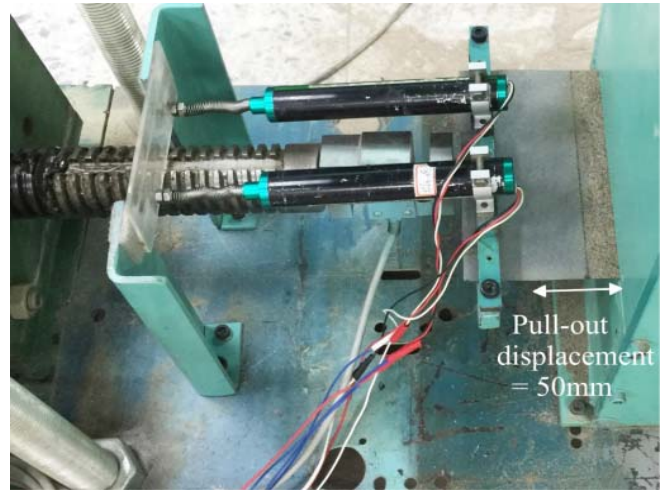
(a) L_t = 50 mm

(a) Completion of sand specimen preparation

(b) L_t = 75 mm

(b) Pull-out failure observed at a large pull-out displacement of 50 mm

(c) L_t = 100 mm

Fig. 4   Pull-out load *vs*. displacement relationships obtained under dry environmental conditions
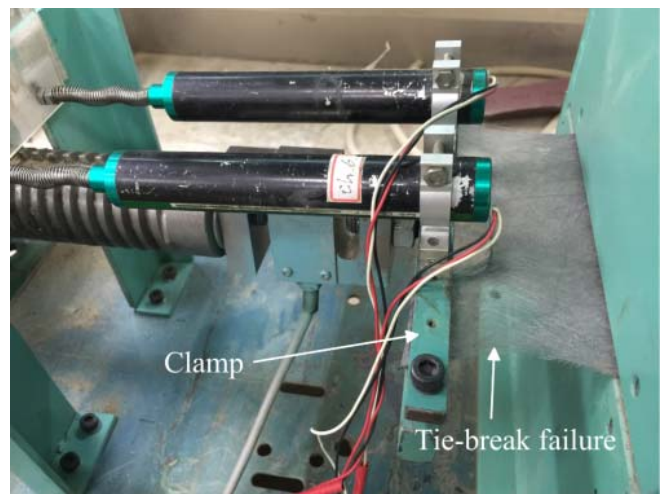
(c) Tie-break failure

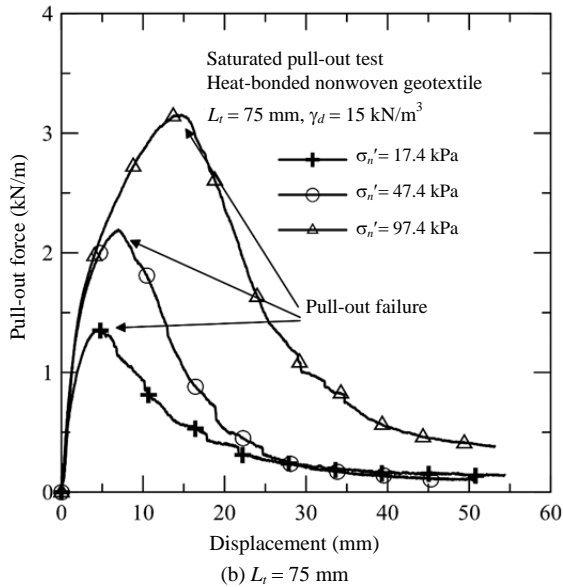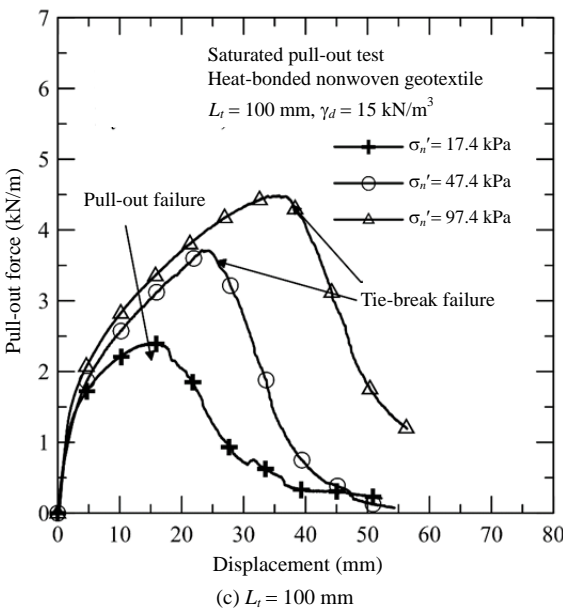**Fig. 5   Typical examples of the pull-out test**
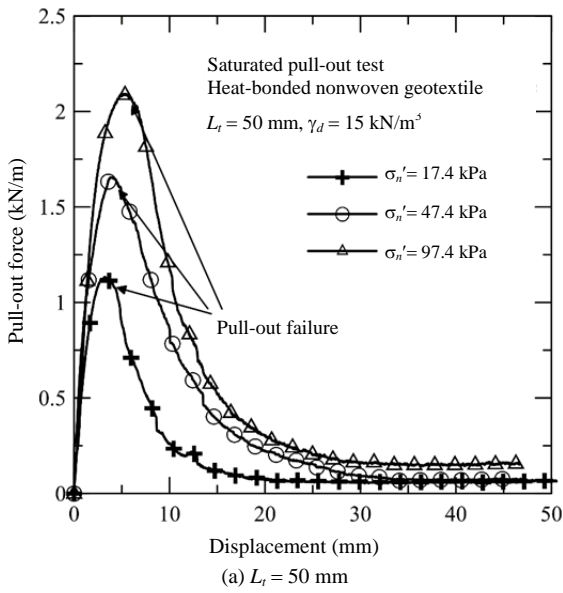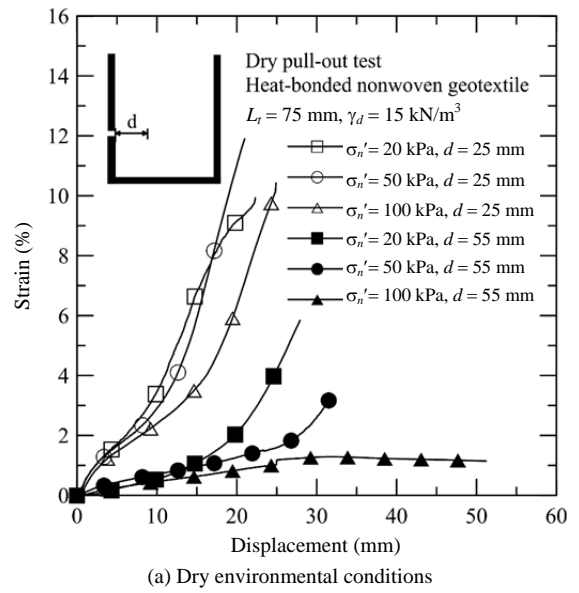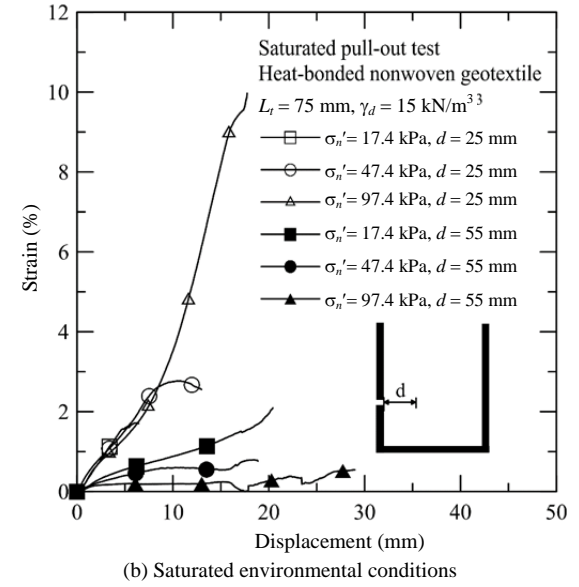
(a) $L_t = 50$ mm

(b) $L_t = 75$ mm

(c) $L_t = 100$ mm

Fig. 6   Pull-out load *vs*. displacement relationships obtained under saturated environmental conditions

(a) Dry environmental conditions

(b) Saturated environmental conditions

Fig. 7   Typical examples of non-uniform tensile strain distributions measured in the case of $L_t = 75$ mm

those in the dry case. However, the group of curves for $d = 55$ mm has a similar trend as that observed for the dry case, except that smaller tensile strains and smaller Δ occur at the moment of abrupt transition as compared to the dry case. Comparing the observations from Figs. 7(a) and 7(b), tensile strains seem to mobilize more effectively in the case of dry sand, in the sense that larger values of tensile strains are associated with larger values of Δ for the dry case as compared to the saturated case, regardless of the value of σ_n'.

6.   RESULTS OF DIRECT SHEAR TESTS ON SAND-GEOTEXTILE INTERFACE

Figure 8 shows a medium-scale direct shear apparatus used for investigating soil-geotextile interface friction characteristics. The shear boxes are 300 mm wide, 300 mm long, and 150 mm high. The upper shear box was rigidly fixed and the lower box is displaced using a precision screw jack with a constant displacement rate of 2 mm/min along two linear rollers. Figure 9(a) shows comparisons of shear stress *vs*. shear displacement
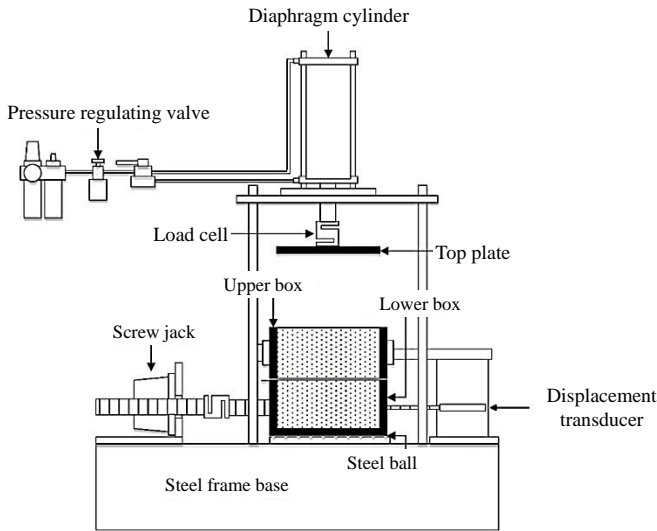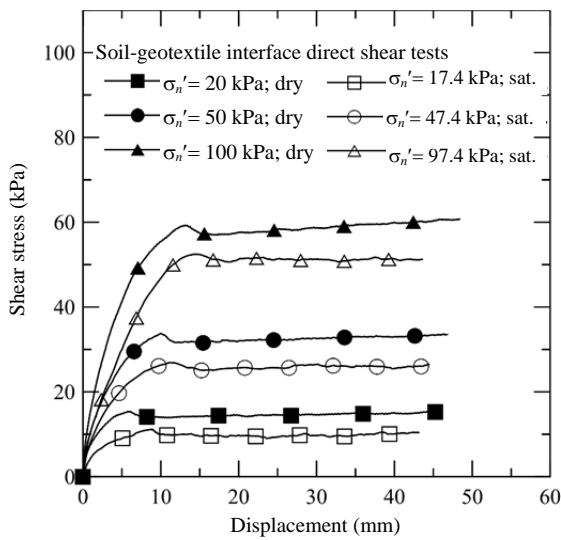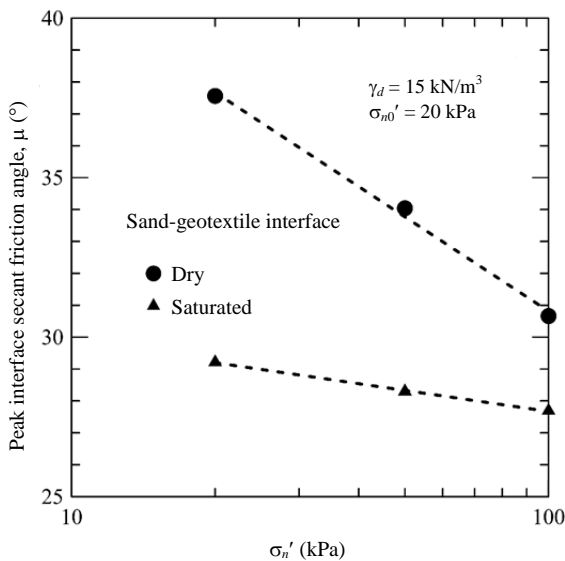
Fig. 8   Side-view of medium-scale direct shear test apparatus

(a) Stress *vs.* displacement relationships

(b) Stress-level-dependency of secant friction angles

Fig. 9   Results of soil-geotextile interface direct shear tests under dry and saturated environmental conditions

curves between dry and saturated conditions in some medium-scale direct shear tests on the soil-geotextile interface. The sand and geotextile used in the direct shear tests are identical to those used in the pull-out tests reported here. It can be seen that the shear stresses obtained for the dry condition are consistently higher than those for the saturated conditions at specific shear displacements. This difference may be due to the lubricant effect of the pore water on the soil-geotextile interface friction. Figure 9(b) shows the stress level dependency of secant interface friction angles (μ) based on the curved failure envelope obtained at peak shear stress conditions shown in Fig. 9(a). These friction angles are logarithmic functions of effective confining stresses, expressed as:

$$\mu = a - b \cdot \log(\sigma'_n / \sigma'_{n0}) \tag{1}$$

where

a = 37.7° and 29.2° for dry and saturated conditions, respectively

b = 9.81° and 2.2° for dry and saturated conditions, respectively

σ_{n0}' : Reference confining stress (= 20 kPa)

σ_n' : Confining stress in the range of 20 to 100 kPa

7.   POREWATER PRESSURE RESPONSE DURING PULL-OUT

Figures 10(a) to 10(c) show typical examples of porewater pressure responses during pull-out tests using L_t = 75 mm under conditions of σ_n' = 20, 50, and 100 kPa, respectively. It can be seen that porewater pressures at the points of d = 150 and 275 mm from the pull-out slit remained almost constant during the test. Only the one at d = 25 mm showed a consistent trend of decreasing porewater pressure, suggesting that negative excess porewater pressures existed at the vicinity of the pull-out slit. This observation is true for all tests regardless of the values of L_t and/or σ_n'. In the following analyses, a porewater pressure of 3.0 kPa was used to derive the effective confining pressures for all the pull-out tests on saturated sands. The small, local negative porewater pressures generated at the vicinity of the pull-out face are ignored.

8.   HYPERBOLIC MODELING FOR PULL-OUT OF GEOTEXTILES

Figure 11 schematically shows a T against Δ relationship based on a hyperbolic model expressed as:

$$T = \frac{\Delta}{a + b \cdot \Delta} \tag{2}$$

$$a = \frac{1}{k_{initial}} \tag{3}$$

$$b = \frac{1}{T_{ult}} = \frac{R_t}{T_f} \tag{4}$$

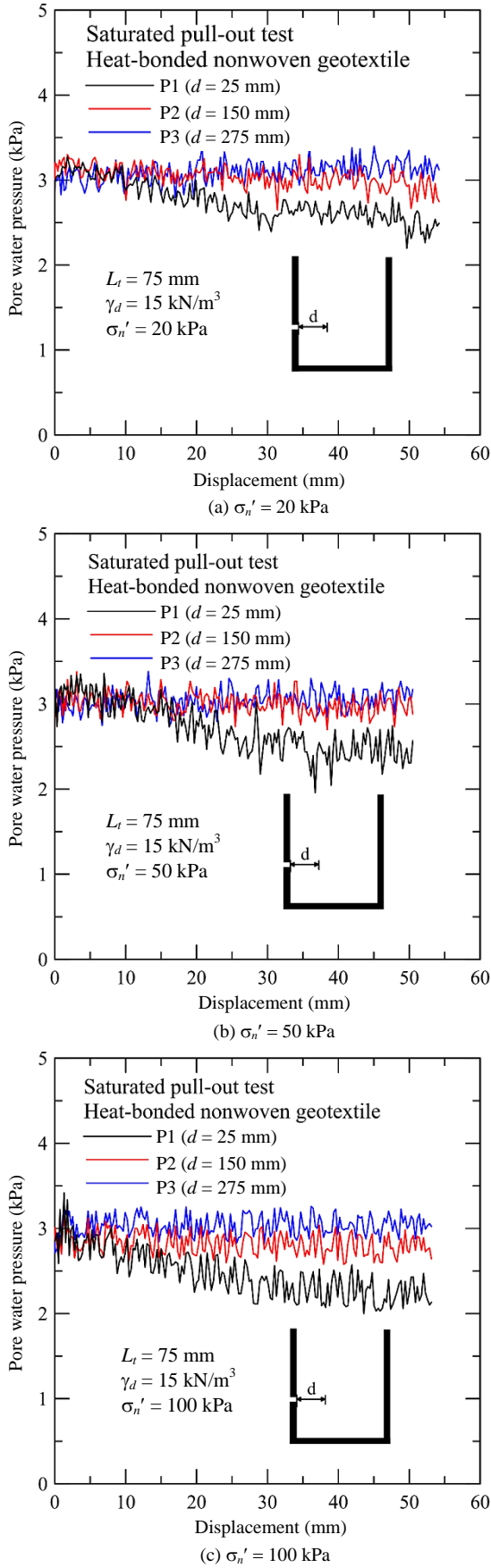$$k_{initial} = K_t \cdot G_t \cdot \left(\frac{\sigma_n}{P_a}\right)^m \tag{5}$$

Fig. 10 Typical examples of excess porewater pressures measured at various locations from the pull-out slit for the case of L_t = 75 mm under various conditions

where

$k_{initial}$	:	Initial shear stiffness (or initial spring constant)
R_t	:	Failure ratio between failure (τ_{fi}) and asymptote shear strength (τ_{ult})
P_a	:	Reference pressure (equal to the atmospheric pressure of 101.3 kPa)
G_t	:	Reference shear stiffness (= 101.3 kPa/m)
K_t	:	Initial shear stiffness number
m	:	Exponent for initial shear stiffness function
T_{ult}	:	Ultimate asymptote pull-out force (= T_f / R_t).

The pull-out force at failure (T_f) is controlled by the smaller peak pull-out resistance (T_p) and breakage tensile force (T_b). In the present study, T_b = 4.1 kN/m, which is determined based on the results of the wide-width tensile test shown in Fig. 3(a); the values of T_p are evaluated based on the following equation:

$$T_p = 2 \cdot L_e \cdot \sigma'_n \cdot \tan \mu \qquad (6)$$

where

L_e	:	Effective pull-out length for which a full mobilization of peak interface friction angles (μ) is assumed, and $L_e \leq L_t$.
σ'_n	:	Effective overburden pressure on the specimen.

It is noted that L_e is a key element for evaluating T_p, which plays a fundamental part in establishing an accurate hyperbolic pull-out model, as shown in Eqs. (2) ~ (4). To obtain the experimental values of L_e, only the tests with pull-out failures (excluding the tests with tensile breakage) were used to back-calculate the values of L_e using Eq. (6). Based on the results of the dry pull-out tests exhibiting pull-out failure mode (a total of 7 tests, as shown in Fig. 12), the back-calculated values of L_e can be expressed as functions of L_t and σ'_n as follows:

$$L_e = -0.11 + 0.99 \cdot L_t + (20.8 - 0.97 \cdot L_t) \cdot \log\left(\frac{\sigma'_n}{\sigma'_{n0}}\right) \qquad (7)$$

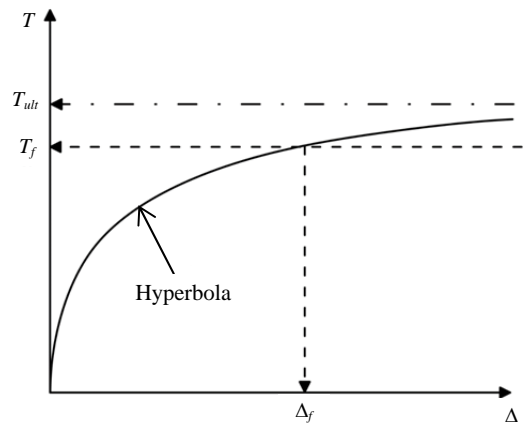**Fig. 11** Scheme of hyperbolic load *vs.* displacement pull-out responses
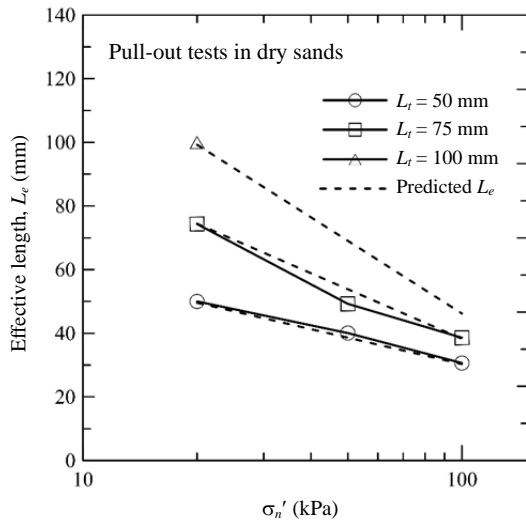
Fig. 12   Comparisons of experimental and fitted values of L_e for the pull-out tests under dry environmental conditions
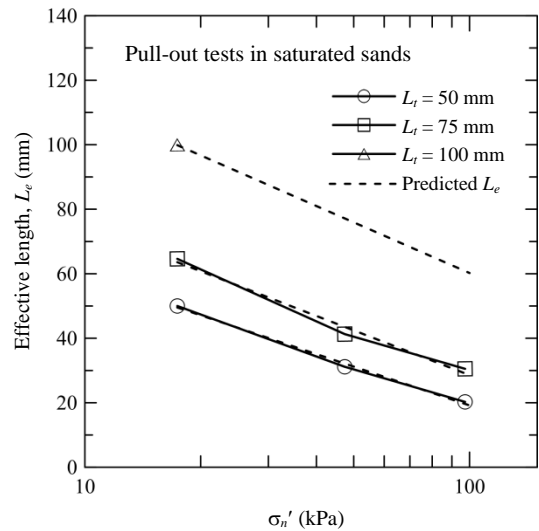

Fig. 13   Comparisons of experimental and fitted values of L_e for the pull-out tests under saturated environmental conditions

where L_e and L_t are in meters, and the value of coefficient of determination (R^2) for Eq. (7) is 0.978. The dotted lines shown in Fig. 12 represent the model-predicted values of L_e using Eq. (7), which showed good fit with the experimental values.

By using similar techniques as those used for deriving Eq. (7) and Fig. 12, the following equation for L_e is derived for the case of saturated sands:

$$L_e = 88.2 - 1.66 \cdot L_t + 0.02 \cdot L_t^2$$
$$+ (-27.8 - 0.24 \cdot L_t) \cdot \log\left(\frac{\sigma_n'}{\sigma_{n0}'}\right) \tag{8}$$

The value of R^2 for Eq. (8) is 0.987. It can be seen from Fig. 13 that Eq. (8) gives an accurate prediction of L_e with negligibly small errors. Comparing Figs. 12 and 13, it can be seen that Eq. (8) gives a more accurate prediction of L_e for the saturated pull-out case as compared to that based on Eq. (7) for the dry case. Although non-uniform tensile strain distributions as shown in Figs. 7(a) and 7(b) were not directly applied in this pull-out model, the simplified approach using effective length (L_e) can greatly reduce the complexity of the model. To take into account the non-uniform strain (or stress) distribution, sophisticate numerical analyses are necessary. However, numerical analyses require additional costs of manpower, computer time, and judgement for the results. A simplified experiment-based model as that proposed here can greatly reduce the above-mentioned costs. Furthermore, the reliability of the proposed model can be improved through more experimental observations in the future.

Regression analyses for the pull-out force *vs.* displacement relationships obtained in the tests on dry sands based on Eqs. (2) ~ (5) were performed. The hyperbolic model parameters K_t, m, and R_t are summarized in Table 1. It can be found that the values of L_t, m, and R_t for the pull-out in dry sands are functions of L_t, expressed as:

$$K_t = 14.0 - 56.2 \cdot L_t \tag{9}$$

$$m = 0.18 - 4.6 \cdot L_t \tag{10}$$

$$R_t = 0.59 + 2.9 \cdot L_t \tag{11}$$

Table 1   Summary of the hyperbolic model parameters obtained from the curve-fitting for the pull-out tests in dry and saturated sands

	L_t (mm)	K_t	m	R_t
Dry sand	50	11.21	−0.06	0.74
	75	9.81	−0.17	0.81
	100	8.40	−0.29	0.89
Saturated sand	50	12.09	0.109	0.65
	75	9.01	−0.067	0.75
	100	5.94	−0.243	0.84

where, L_t is in meters, and the value of R^2 for Eqs. (9), (10) and (11) are 0.963, 0.951 and 0.802, respectively. A similar regression analysis is performed for the results of the pull-out tests on saturated sands. The hyperbolic model parameters for the pull-out in saturated sands are also summarized in Table 1, expressed as functions of L_t (in meters):

$$K_t = 18.2 - 123.1 \cdot L_t \tag{12}$$

$$m = 0.46 - 7.04 \cdot L_t \tag{13}$$

$$R_t = 0.46 + 3.8 \cdot L_t \tag{14}$$

The value of R^2 for Eqs. (12), (13), and (14) are 0.999, 1.0 and 0.999, respectively. Figures 14(a) to 14(c) show the hyperbolic model parameters, K_t, m, and R_t for both the dry and saturated cases. For both of these cases, a trend of decreasing K_t with the increase in L_t can be seen, suggesting a decrease of pull-out stiffness with increasing lengths of pull-out specimens. This is because the overall pull-out displacement contributed by the integrated tensile strains along the specimen increases as the length of the specimen increases. It can also be seen that the values of K_t are generally smaller in the saturated cases than those in the dry ones, except those in the case of $L_t = 50$ mm in which the state of the soil saturation seems to have a negligible effect on the value
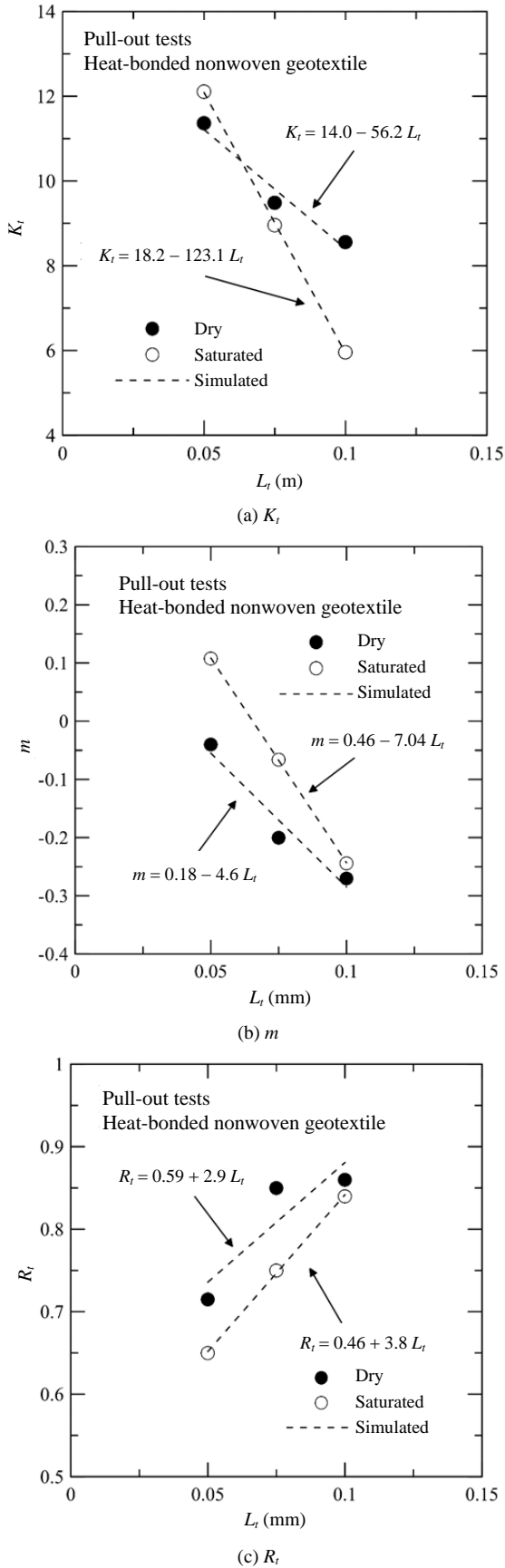
(a) K_t

(b) m

(c) R_t

Fig. 14   Comparisons of hyperbolic pull-out model constants against embedment length (L) of reinforcement under dry and saturated conditions

of K_t. Figure 14(b) shows that soil saturation generally results in higher values of m than those in the dry case, suggesting that smaller values of initial pull-out stiffness ($k_{initial}$) are for the saturated cases as compared to those in the dry cases. The descending trend of m against the increase of L_t suggests that the relative influences of confining pressures on the values of $k_{initial}$ increase with increases in L_t. Figure 14(c) shows that similar trends of R_t *vs.* L_t relationships are obtained in both dry and saturated cases. In addition, the values of R_t for the saturated cases are generally smaller than those for the dry cases, suggesting that smaller pull-out displacement at failure conditions occurs under saturated conditions as compared to under dry conditions.

9.   COMPARISONS BETWEEN MEASURED AND MODEL-PREDICTED PULL-OUT RESPONSES

Figures 15(a) to 15(c) show comparisons of the experimental and model-predicted T *vs.* Δ relationships for $L_t = 50$, 75, and 100 mm, respectively, under dry conditions. For the case of $L_t = 50$ mm, both the failure mode, the T-Δ curves, and the T_f are well-predicted. For the case of $L_t = 75$ mm, the ultimate pull-out force for the two cases with relatively low confining pressures that failed under the pull-out mode are also well-predicted. In addition, the tie-break failure that occurred for the case of $\sigma_n' = 100$ kPa is also well-predicted, in the sense that the predicted peak value of the pull-out force is slightly greater than the experimental one controlled by the tie-break of the specimen.

Figures 16(a) to 16(c) compare the model-predicted and the experimental pull-out responses for $L_t = 50$, 75, and 100 mm conditions, respectively, under saturated conditions. Figures 16(a) and 16(b) both show that the hyperbolic model-generated T-Δ curves agreed well with the measured ones. For the case of $L_t = 100$ mm, as shown in Fig. 16(c), the hyperbolic model succeeded in predicting the pull-out behavior for the case with a low confining pressure of $\sigma_n' = 20$ kPa. However, it failed to predict the pull-out response for the cases with relatively high confining pressures of $\sigma_n' = 50$ and 100 kPa which exhibited a tie-break failure mode. For these two cases, the model predicted tie-break failures to occur at some values of Δ smaller than the measured ones. This is true for both the dry and saturated cases (see Figs. 15(c) and 16(c)). The underestimation of Δ at the moment of the tie-break failures may be due to the relatively extensible properties at tensile strains $\varepsilon_t > 5\%$, as shown by the stress-strain relationships for the geotextile in Fig. 3(a). For a specimen at the verge of tie-break failure, the tensile elongation at the vicinity of the clamp may become dominant, *i.e.*, the pull-out displacement generated by the slippage of the geotextile-sand interface is overwhelmed by the tensile elongation of the pull-out specimen around the grip-sand interface. This mechanism is not taken into account in the present hyperbolic model. The extraordinary tensile elongations of the geotextile at the verge of tie-break failure have yet to be considered in the near future. Note that the derived formulae are preliminarily verified here using the experimental data which were used in the regression analysis. The general applicability of the proposed formulae should be examined in the near future based on new experimental data for wide varieties of material and test conditions.
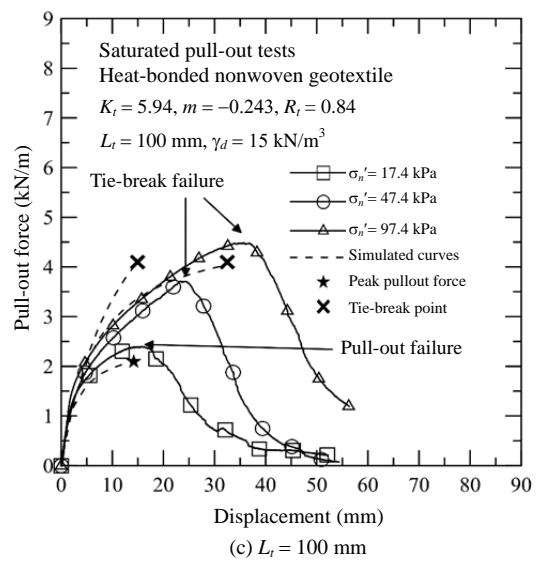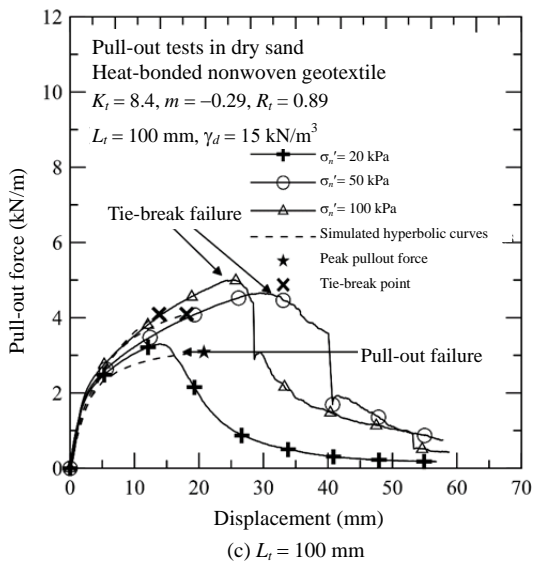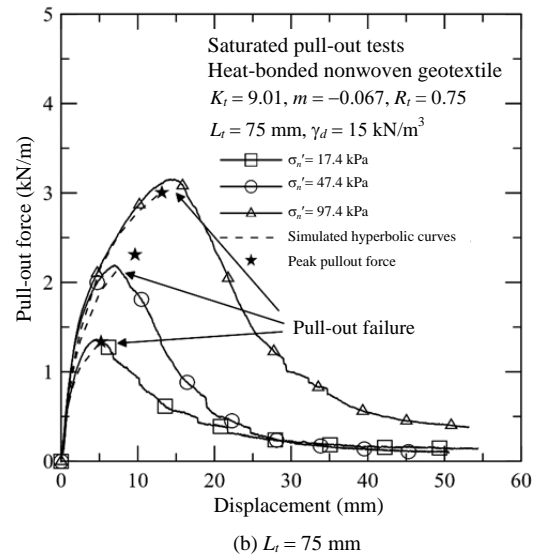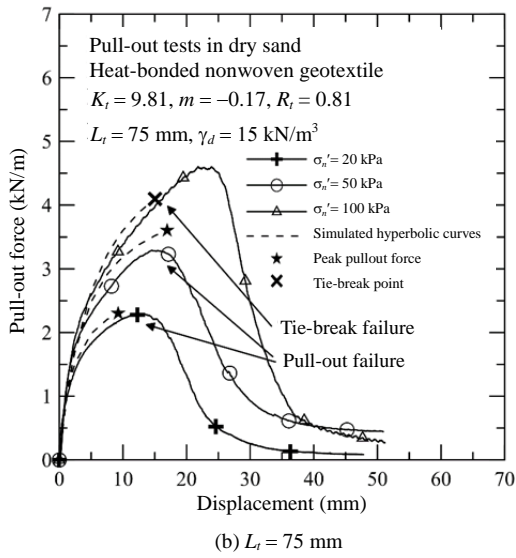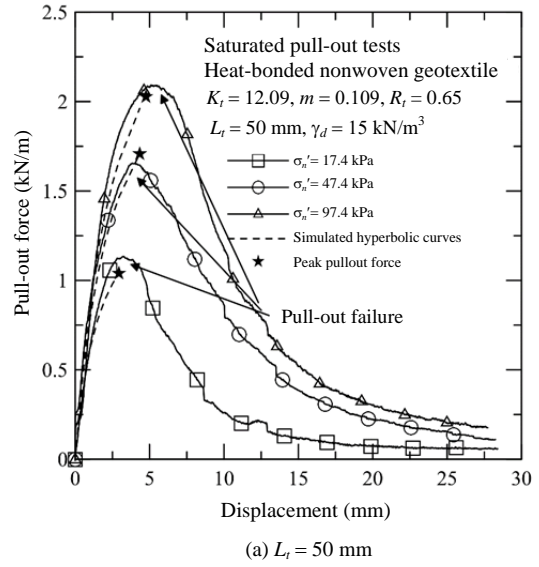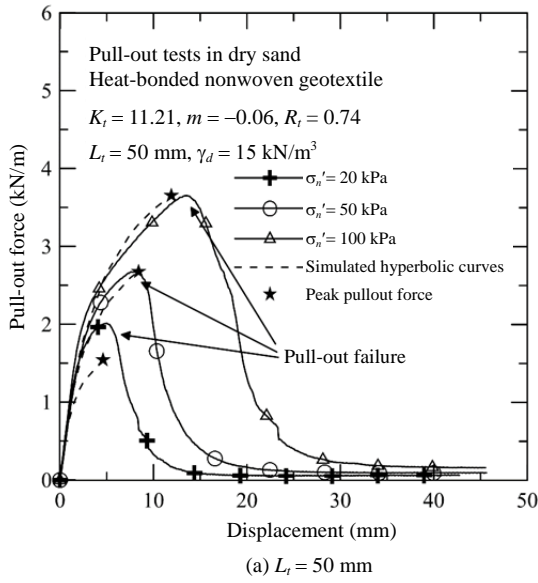
Fig. 15   Comparisons of the measured and model-predicted pull-out force-displacement relationships based on the test results under dry environmental conditions

Fig. 16   Comparisons of the measured and model-predicted pull-out force-displacement relationships based on the test results under saturated environmental conditions

10. CONCLUSIONS

A series of pull-out tests on a heat-bonded nonwoven geotextile was conducted using silty sand under both dry and saturated conditions. To investigate possible differences in the pull-out behavior induced by saturating the soil and pull-out specimens, hyperbolic models for pull-out resistance (T) *vs.* pull-out displacement (Δ) were established based on the experimental results. Under otherwise similar testing conditions, the pull-out of the heat-bonded nonwoven geotextile in a saturated sandy medium exhibits smaller peak pull-out force (T_f) and smaller pull-out displacement at peak pull-out force (Δ_f), as compared with those under dry conditions. Observations of the pull-out behavior during the tests showed that the tensile strain (and/or stress) distributions along the geotextile are always non-uniform. Therefore, an accurate evaluation of the effective (or active) pull-out lengths (L_e) is fundamentally important for accurate modeling of the pull-out behavior of geotextiles. It was shown that the effective pull-out length of the tested geotextile is a polynominal function of the embedment length (L_t) as well as a logarithmic function of the confining pressures (σ_n'). Based on the regression analyses of the experimental results, the stiffness number (K_t) is higher for the dry case than it is for the saturated one. However, the differences diminish in the cases of short specimen lengths; the stress level dependency exponent (m) is greater in the saturated case than it is in the dry one, suggesting that the initial pull-out stiffness ($k_{initial}$) in the saturated case is more sensitively affected by the change of stress levels than it is in the dry case; the peak-to-ultimate pull-out strength ratio (R_t) is greater in the dry case than it is in the saturated one, suggesting that the peak strength for the dry case occurred in a smaller pull-out displacement than it did in the saturated case. However, the differences in m and R_t in the dry and saturated cases diminish at a confining pressure of 100 kPa, which is a relatively high confining pressure used in the present study.

REFERENCES

ASTM International, *ASTM D2487. Standard Practice for Classification of Soils for Engineering Pruposes (Unified Soil Classification System)*. West Conshohocken, PA, USA.

ASTM International, *ASTM D4595. Test Methods for Tensile Properties of Geotextiles by the Wide-Width Strip Method*. West Conshohocken, PA, USA.

ASTM International, *ASTM D6706. Standard Test Method for Measuring Geosynthetic Pullout Resistance in Soil*. West Conshohocken, PA, USA.

Bacas, B.M., Canizal, J., and Konietzky, H. (2015). "Frictional behaviour of three ciritical geosynthetic interfaces." *Geosynthetics International*, **22**(5), 355–365.

Berg, R.R., Barry, P.E., and Christopher, R. (2009). *Design and Construction of Mechanically Stabilized Earth Walls and Reinforced Soil Slopes*, Volume 1, Publicaton No. FHWA-NHI-10-024, FHWA GEC 011-Volume 1, U.S. Department of Transportation, Federal Highway Administration.

Ferreira, F.B., Vieira, C.S., and Lopes, M.L. (2015). "Direct shear behaviour of residual soil-geosynthetic interfaces-influence of soil moisture content, soil density and geosynthetic type." *Geosynthetics International*, **22**(3), 257–272.

Gardile, G., Moraci, N., and Calvarano, L.S. (2016). "Geogrid pullout behaviour according to the experimental evaluation of the active length." *Geosynthetics International*, **23**(3), 194–205.

Huang, C.-C. (2016a). "Ultimate bearing capacity of saturated reinforced horizontal ground." *Geosynthetics International*, **23**(1), 1–8.

Huang, C.-C. (2016b). "Settlement of footings at the crest of reinforced slopes subjected to toe unloading." *Geosynthetics International*, **23**(4), 247–256.

Huang, C.-C., Hsieh, H.-Y., and Hsieh, Y.-L. (2014). "Hyperbolic models for a 2-D backfill and reinforcement pullout." *Geosynthetics International*, **21**(3), 168–178.

Huang, C.-C., Lo, C.-L., Jang, J.-S., and Hwu, L.-K. (2008). "Internal soil moisture response to rainfall-induced slope failures and debris discharge." *Engineering Geology*, **101**(3-4), 134–145.

Huang, C.-C., Ju, Y.-J., Hwu, L.-K., and Lee, J.-L. (2009). "Internal soil moisture and piezometric responses to rainfall-induced shallow slope failures." *Journal of Hydrology*, **370**(1-4), 39–51.

Krahn, T., Blatz, J., Alfaro, M., and Bathurst, R.J. (2007). "Large-scale interface shear testing of sandbag dyke materials." *Geosynthetics International*, **14**(2), 119–126.

Liu, C.-N., Zornberg, J.G., Chen, T.-C., Ho, Y.-H., and Lin, B.-H. (2009). "Behavior of geogrid-sand interface in direct shear mode." *Journal of Geotechnical and Geoenvironmental Engineering*, ASCE, **135**(12), 1863–1869.

Palmeira, E.M. (2009). "Soil-geosynthetic interaction: Modellig and analysis." *Geotextiles and Geomembranes*, **27**(4), 368–390.

Pathak, Y.P. and Alfaro, M.C. (2010). "Wetting-drying behavior of geogrid-reinforced clay under working load conditions." *Geosynthetics International*, **17**(3), 144–156.

Pinho-Lopes, M., Paula, A.M., and Lopes, M.L. (2015). "Pullout response of geogrids after installation." *Geosynthetics International*, **22**(5), 339-354.

Portelinha, F.H.M., Bueno, B.S., and Zornberg, J.G. (2013). "Performance of nonwoven geotextile-reinforced walls under wetting conditions: Laboratory and field investigations." *Geosynthetics International*, **20**(2), 90–104.

Shukla, S.K. (2002). *Fundamentals of Geosynthetics. In Geosynthetics and Their Applications,* Shukla, S.K. Ed., Thomas Telford, London, UK, 1–54.

Vieira, C.S., Lopes, M.L., and Caldeira, L.M. (2013). "Sand-geotextile interface characterization through monotonic and cyclic direct shear tests." *Geosynthetics International*, **20**(1), 26–38.

Verira, C.S. and Pereira, P.M. (2015). "Interface shear properties of geosynthetics and construction and demolition waste from large-scale direct shear tests." *Geosynthetics International*, **23**(1), 62–70.

Weerasekara, L. and Wijewichreme, D. (2010). "An analytical method to predict the pullout response of geotextiles." *Geosynthetics International*, **17**(4), 193–206.

Yang, K.-H., Zornberg, J.G., and Lin, H.-D. (2012). "Stress distribution and development within geosynthetic-reinforced soil slopes." *Geosynthetics International*, **19**(1), 62–78.

Yang, K.-H., Nguyen, M.D., Mengist, W., Liu, C.N., and Gupta, R. (2016). "Behavior of geotextile-reinforced clay under consolidated undrained tests: reinterpretation of porewater pressure parameters." *Journal of GeoEngineering*, **11**(2), 33–45.